Two-particle Aharonov–Bohm effect in electronic interferometers

2010 J. Phys. A: Math. Theor. 43 354027

(http://iopscience.iop.org/1751-8121/43/35/354027)

J. Phys. A: Math. Theor. **43** (2010) 354027 (9pp) doi:10.1088/1751-8113/43/35/354027

Two-particle Aharonov–Bohm effect in electronic interferometers

Janine Splettstoesser[1,2], **Peter Samuelsson**[3], **Michael Moskalets**[4] **and Markus Büttiker**[5]

[1] Institut für Theoretische Physik A, RWTH Aachen University, D-52056 Aachen, Germany
[2] JARA—Fundamentals of Future Information Technology, Germany
[3] Division of Mathematical Physics, Lund University, Box 118, S-221 00 Lund, Sweden
[4] Department of Metal and Semiconductor Physics, NTU 'Kharkiv Polytechnic Institute', 61002 Kharkiv, Ukraine
[5] Département de Physique Théorique, Université de Genève, CH-1211 Genève 4, Switzerland

E-mail: splett@physik.rwth-aachen.de

Received 26 February 2010, in final form 18 May 2010
Published 12 August 2010
Online at stacks.iop.org/JPhysA/43/354027

Abstract
We review recent theoretical investigations on the two-particle Aharonov–Bohm effect and its relation to entanglement production and detection. The difficulties of the entanglement detection due to dephasing and finite temperature are discussed regarding a recent experimental realization of a two-particle Aharonov–Bohm interferometer [15]. We also discuss a theoretical proposal for a two-particle Aharonov–Bohm interferometer, which as against the finite bias setup is driven with dynamical single-electron sources allowing for the tunable production of time-bin entanglement.

PACS numbers: 72.10.−d, 73.23.−b, 72.70.+m

(Some figures in this article are in colour only in the electronic version)

1. Introduction

The Aharonov–Bohm (AB) effect [1] played a central role in the development of mesoscopic physics. Much of this initial theoretical [2] and experimental [3] work focused on samples with a ring geometry to detect the single-particle quantum interference in response to an AB flux. Beyond the *single-particle* interference, the *two-particle* interference effects are quantum mechanical phenomena of particular interest. They are known from examples in optics, such as the Hanbury Brown–Twiss effect [4] and the Hong–Ou–Mandel [5] effect. Two-particle correlations with massive particles in the form of current–current correlations in mesoscopic multiprobe electrical conductors have been discussed by Büttiker [6] and Martin and Landauer [7] and have been experimentally investigated by Oliver *et al* [8] and Henny *et al* [9]. More

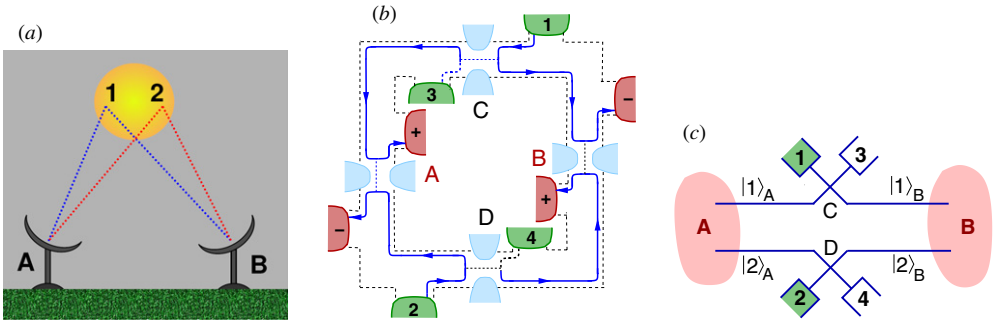

Figure 1. (*a*) Schematic of the original optical HBT intensity interferometer designed to measure the angular diameter of stars, from [17]. (*b*) Implementation of a fermionic two-particle interferometer in the quantum Hall regime, from [14]. (*c*) Schematic of the source part of the 2PI, from [17].

recently bunching and anti-bunching phenomena have found interest in cold-atom physics [10, 11]. In recent years much interest has been on the generation, manipulation and detection of entanglement, which is a resource for quantum information processes. There is indeed an intimate relation between two-particle interference and entanglement in the two-particle interferometer [12] (2PI). Here, it is thus not single-particle interference that counts, but as we explain in this article, a two-particle AB effect is the center of interest.

Complex electronic interferometers (in analogy to optical ones) are conveniently realized in conductors in the quantum Hall regime [13] where electrons propagate along chiral edge states. In mesoscopic physics electrons can play a similar role as photons do in optics: chiral edge states take the role of waveguides and quantum point contacts (QPCs) constitute beam splitters having a controllable transmission. A 2PI showing the two-particle AB effect was recently proposed theoretically [14] and realized experimentally [15]. It is therefore of deep interest to find out about the possibilities of entanglement production and detection in the presence of dephasing and finite temperature [16, 17]. Early works [18] and related ideas for a two-particle AB effect are presented in [19, 20].

The recent experimental success in implementing a high-frequency single-electron source in the integer quantum Hall regime [21, 22] triggered the idea to design 2PIs, which are based on the tunable emission of *single* electrons or holes from different sources into the interferometer setup [23–25]. In a suggested setup, two-particle correlations, appearing as a consequence of erasing of which-path information, manifest themselves as an AB effect in the noise. This goes along with a tunable time-bin entanglement allowing for entanglement on demand.

2. Entanglement production and detection at finite temperatures

An electronic analog to the optical Hanbury Brown–Twiss interferometer (HBT) [4], shown in figure 1(*a*), was theoretically proposed in [14]. This proposal envisaged a setup in the integer quantum Hall regime, see figure 1(*b*), including four uncorrelated sources of which sources 3 and 4 are grounded and a bias V is applied to sources 1 and 2. Particles emitted from the sources into chiral edge states (solid lines in figure 1(*b*)) are scattered at QPCs with transmissions t_A, t_B, t_C, t_D before they are detected at one of the four detector contacts $A\pm$ and $B\pm$. Transmission t and reflection r are defined following the logic of figure 1(*c*). The setup is penetrated by a magnetic flux Φ. While the geometry prohibits the appearance of single-particle interference, measurable in the current, two-particle interferences can be detected.

The joint probability to measure a particle in the detector $A\alpha$ and at the same time a particle in the detector $B\beta$, with $\alpha = \pm$ and $\beta = \pm$, is given by

$$\begin{aligned} P_{A\alpha B\beta}(0) &\propto |s_{A\alpha 1}s^*_{B\beta 1} + s_{A\alpha 2}s^*_{B\beta 2}|^2 + (|s_{A\alpha 1}|^2 + |s_{A\alpha 2}|^2)(|s_{B\beta 1}|^2 + |s_{B\beta 2}|^2) \\ &\propto S_{A\alpha B\beta} + 2\tau_C I_{A\alpha} I_{B\beta}, \end{aligned} \tag{1}$$

with the coherence time τ_C depending on voltage and temperature. The joint probability can be expressed by the average currents $I_{A\alpha}$ and $I_{B\beta}$ into the detectors and by the zero-frequency current–current correlator $S_{A\alpha B\beta}$ between currents detected at $B\pm$ and $A\pm$ [26]. For the simple case of semitransparent QPCs and energy-independent scattering amplitudes, these long-time observables are given by

$$I_{A\alpha} = I_{B\beta} = \frac{e^2 V}{2h}, \qquad S_{A\alpha B\beta} = \frac{e^3 V}{4h}[1 + \alpha\beta\cos\phi]. \tag{2}$$

The flux-dependence of the current–current correlator is the signature of the two-particle AB effect. The magnetic flux Φ enters through the corresponding phase $\phi = 2\pi\Phi/\Phi_0$, with $\Phi_0 = h/e$ being the single-particle flux quantum.

The connection between the two-particle AB effect and orbital entanglement can be seen from the examination of the many-body ground state of the electrons injected into the interferometer. The initial state of injected particles at zero temperature is given by $|\Psi_{\rm in}\rangle = \prod_{0\leqslant E\leqslant eV} a_1^\dagger(E)a_2^\dagger(E)|\bar{0}\rangle$, where $a_1^\dagger(E)$ creates an electron with energy E incident from source 1 on the filled Fermi sea $|\bar{0}\rangle$. For the projection of the outgoing state on the part with one particle reaching the beam splitter A and one particle reaching the beam splitter B coming either from source 1 or 2, one obtains

$$|\Psi_{AB}(E)\rangle = \frac{1}{\sqrt{N}}\left(r_C t_D b^\dagger_{A1} b^\dagger_{B2} - r_D t_C b^\dagger_{A2} b^\dagger_{B1}\right)|\bar{0}\rangle \tag{3}$$

using the scattering matrices of the different beam splitters; an operator $b^\dagger_{A1}$ creates an electron close to the beam splitter A on the upper half of the setup. N is a normalization constant. The entanglement of the state $|\Psi_{AB}(E)\rangle$ can conveniently be quantified in terms of the concurrence C [27], which ranges from zero for an unentangled state to unity for a maximally entangled state. Indeed we find for $|\Psi_{AB}\rangle$ the concurrence

$$C = \frac{2}{N}|r_C t_C r_D t_D| = \frac{2}{N}\sqrt{R_C T_C R_D T_D} \tag{4}$$

which reaches unity for semitransparent beam splitters. Note that the normalization factor N is then maximal, namely equal to $1/2$. This demonstrates that at most only half of the particles injected from 1 and 2 lead to split pairs, with one particle emitted toward A and one toward B, i.e. a maximal pair emission probability of $1/2$. For a measurement during a time τ the maximum concurrence production [28] is thus $\mathcal{N}/2$, where $\mathcal{N} = \tau eV/h$ is the number of pairs injected from 1 and 2 in the time τ and in the energy interval $0 \leqslant E \leqslant eV$.

Indeed the two-particle AB effect was experimentally realized [15] in the above suggested spirit. By electrical gating both the situation in which single-particle interference is visible and the situation where single-particle interference is fully suppressed were obtained. Magnetic-field-dependent interference patterns in the current crosscorrelations were measured in the latter case, which could clearly be attributed to the two-particle AB effect. The experiment showed an amplitude suppression of the two-particle AB effect to 25% of the theoretically predicted value due to finite temperature and dephasing. This demands for a theory for entanglement generation, characterization and detection in fermionic 2PIs at finite temperature and finite dephasing. The question is if the electrons reaching the detectors A and B are entangled and, if so, if one can unambiguously detect this two-particle entanglement

by measurements of currents and current correlators—the standard quantities accessible in electronic transport measurements. Both questions were answered positively in [16, 17] as discussed in the following. The effect of dephasing can be modeled by a voltage probe [30] coupled to an interferometer arm, the coherence being quantified by $0 \leqslant \gamma \leqslant 1$, and it can be cast by a suppression factor in the off-diagonal elements of the density matrix $|\Psi_{AB}\rangle\langle\Psi_{AB}|$. The result is a concurrence $C = \gamma$, where we assumed zero-temperature and semitransparent beam splitters, showing that the entanglement persists even for strong dephasing.

The effect of finite temperature is that the injected state is in a mixed state and that in principal all four sources—even the grounded ones—can emit particles. This leads to situations where 0–4 particles are emitted at the same energy and in particular a state having a particle at detector A, and a particle at detector B can have additional electrons at both detectors. It is therefore useful to discuss the entanglement generation and detection in terms of *projected* and *reduced* density matrices from which a *projected* and a *reduced* concurrence can be extracted. The projected density matrix, $\rho_{\mathrm{p}}(E) = \prod_A \otimes \prod_B \rho(E) \prod_A \otimes \prod_B$, is obtained from the full energy-resolved density matrix $\rho(E)$ of the injected state by projecting out the states which have a particle at detector A and B by projection operators $\prod_A$ and $\prod_B$. Finite temperature leads to an overall modification of the energy-dependent probability for two-particle emission via a prefactor containing the Fermi functions of all four sources. Furthermore, equivalent to the effect of dephasing, a suppression of the off-diagonal components appears. Finally, a finite amplitude for the diagonal density matrix elements for two particles being emitted from either sources 1, 3 or 2, 4 is found which is absent at zero temperature. The resulting concurrence shows that entanglement persists up to a certain critical temperature, T_c^p, depending on the coherence γ, the beam splitter transmissions and the applied voltage,

$$kT_c^p = eV \ln\left(\frac{\sqrt{1+4\gamma\sqrt{R_C T_C R_D T_D}}+1}{\sqrt{1+4\gamma\sqrt{R_C T_C R_D T_D}}-1}\right). \tag{5}$$

In particular this shows that in the experiment [15], entanglement was present, i.e. the temperature was below the critical temperature.

Anyhow, experimentally the projected density matrix is not accessible, because in experiment also those states contribute to current and current correlations, which have two particles at the same detector. Furthermore, a current measurement provides in general energy-integrated results. Therefore, it is useful to study the reduced two-particle density matrix also. If one had access to energy filters, the reduced energy-resolved density matrix of the outgoing state with the matrix elements $\left[\rho_r^E\right]_{ij,kl} = \left\langle b_{Ai}^\dagger b_{Bj}^\dagger b_{Bk} b_{Al}\right\rangle$ (where an operator $b_{Ai}^\dagger$ creates an electron in the detector Ai) would be tomographically reproducible by current and current-correlation measurements. The qualitative difference between the energy-resolved reduced and the projected density of states arises from the fact that also states with more than one particle at A and/or B contribute to ρ_r^E but not to $\rho_p(E)$. A crucial result is that the obtained reduced concurrence is always smaller than the projected one. Importantly, at finite temperature, without any energy filters, we do not have access to the energy-resolved quantities discussed above, only to the total currents and current correlators measured at contacts $A\alpha$, $B\beta$. When studying the total reduced density matrix and the extracted concurrence, one finds that only in certain parameter regimes can the reduced concurrence serve as a lower bound to the actual entanglement captured in the projected concurrence. In a regime where this is the case, the reduced and the projected concurrence are shown in figure 2. Even though the corresponding parameter regime was reached in the experiment and the measured reduced concurrence can therefore serve as a lower bound to entanglement, it turns out that the reduced concurrence extracted from measurement is negligibly small and no conclusive statement can therefore be made regarding the experimental entanglement detection in [15]. At the same time these

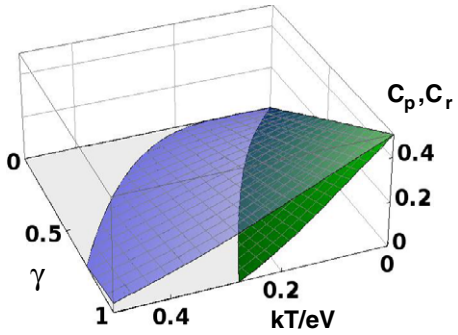

Figure 2. Reduced (lower, green) and projected (upper, blue) concurrence as a function of dephasing and temperature [16].

theoretical findings suggest that by a mere reduction of the temperature, the produced orbital entanglement will be detectable.

3. Tunable time-bin entanglement from single-particle sources

Recently, a single electron source was experimentally realized in the integer quantum Hall regime at gigahertz frequencies [21]. In a controlled manner, by an external driving of electric fields, single electrons and single holes are emitted from such a source close to the lead's Fermi energy. The controlled emission of single particles also allows for controllability in two-particle experiments. Another advantage is that the use of controllable single-particle sources could be a solution to avoid undesirable contribution of the grounded contacts at non-zero temperatures. This is because the contribution of a particle emission from all the contacts is the same with or without working single-particle sources and it constitutes a background which is later subtracted. Here we propose a mesoscopic circuit in the quantum Hall effect regime containing driven single-particle sources; no bias is applied across the device. The proposed setup comprises two uncorrelated single-particle sources and two distant Mach–Zehnder interferometers, with magnetic fluxes. We show that this allows us in a controllable way to produce orbitally entangled electrons while the current is insensitive to magnetic fluxes.

A mesoscopic two-particle collider [23], which is similar to the Hong–Ou–Mandel optical interferometer [5], see figure 3, is at the basis of the more complicated setup mentioned above, showing a two-particle AB effect. In such an electronic Hong–Ou–Mandel interferometer, tunable two-particle correlations are manifest as will be discussed in the following. A mesoscopic cavity—indicated by A or B—is driven by a time-dependent gate potential, yielding the periodical high-frequency emission of the quantized charge. In this setup, the *single* particles (electrons and holes) are injected into edge states and are scattered at QPCs. In the setup shown in figure 3 the two mesoscopic capacitors A and B are contacted by QPCs, with the reflection (transmission) coefficients r_A (t_A) and r_B (t_B), to chiral edge states. The capacitors serving as single-particle sources are driven by the time-dependent potentials $U_A(t)$ and $U_B(t)$, with equal frequency Ω. The emitted particles are transmitted or reflected at the central QPC (C), with the reflection (transmission) coefficients r_C (t_C) before they reach the contacts 1 and 2. If the sources are driven such that the two particles arrive at the quantum point contact independently, they generate the shot noise $\mathcal{P}_{12}$ which—depending on the particle number emitted per period from both sources—is found to be an integer multiple of $\mathcal{P}_0 = -(2e^2/\pi)T_C R_C \Omega$. $\mathcal{P}_0$ is the shot noise produced by the central QPC alone and is independent of the source properties. However, when two particles of the same kind meet at

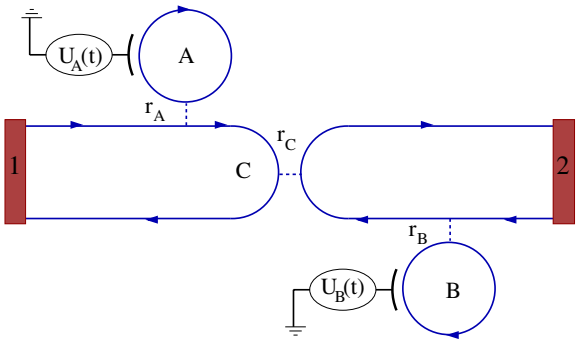

Figure 3. Single particles are emitted from the two capacitors A and B (indicated by circles) through quantum point contacts (indicated as dashed lines) into edge states (indicated by full lines), where they can possibly collide at the central quantum point contact C [23].

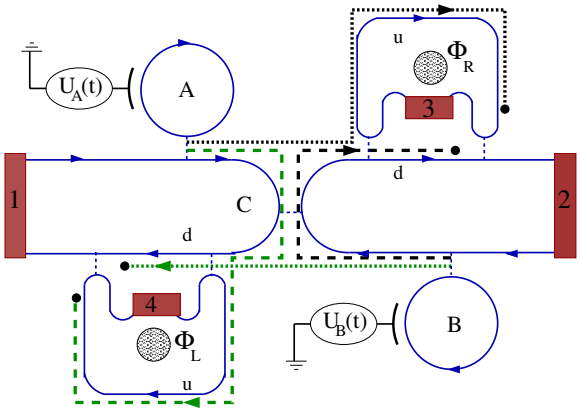

Figure 4. Emitters A and B driven by the potentials $U_A(t)$ and $U_B(t)$ inject single particles into edge states (solid lines). After scattering at a center, QPC (C) particles reach Mach–Zehnder interferometers with the Aharonov–Bohm fluxes Φ_L and Φ_R. The black and grey (green), dotted and dashed lines show possible two-particle trajectories which lead to particle collisions erasing which-path information [25].

the middle QPC, noise suppression is found due to the Pauli principle. In other words, one can see the effect of the fermionic statistics. This setup is the basis for the design of a two-particle emitter with a controllable degree of correlations.

In the following we discuss a setup which is adequate to explore the entanglement production from two uncorrelated sources. For this purpose, we extend the mesoscopic circuit in the quantum Hall effect regime comprising two independent single-particle sources mentioned before by two distant Mach–Zehnder interferometers (MZIs,) with magnetic fluxes [25], as shown in figure 4. Therefore, before reaching the contacts 1–4, the signals from the single-particle sources traverse the lower (d) or upper (u) arms of two MZIs, L and R, pierced by the magnetic fluxes Φ_L and Φ_R. Some of the possible trajectories that a particle can take from one of the sources to one of the contacts are indicated in figure 4.

We consider a model of a mesoscopic capacitor consisting of a single circular edge state [21, 22, 29]. Using a scattering matrix approach, the mesoscopic capacitors, $\alpha = A, B$, with

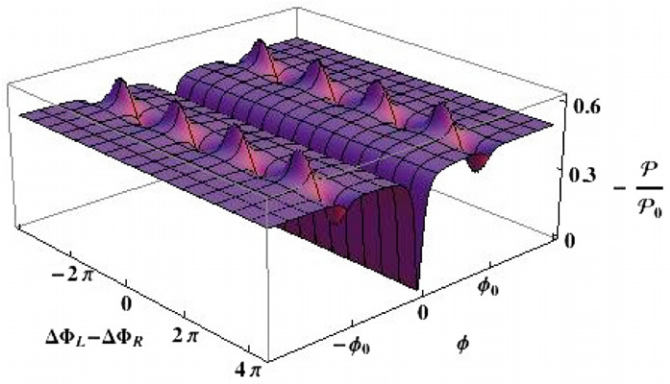

Figure 5. Two-particle Aharonov–Bohm oscillations in the shot-noise correlation $\mathcal{P}_{12}$ as a function of the difference in the magnetic fluxes $\Phi_A - \Phi_B$ and difference of phase φ of the potentials $U_A(t)$ and $U_B(t)$. This phase difference is related to the tunable difference in the emission times from the two cavities [25].

the time-dependent potential $U_\alpha(t)$ are described by a Fabry–Perot-like amplitude [31],

$$S_\alpha(t, E) = r_\alpha + t_\alpha^2 \sum_{q=1}^{\infty} {r_\alpha}^{q-1} \, \mathrm{e}^{\mathrm{i}qE\tau_\alpha - \mathrm{i}\Phi_\alpha^q(t)}, \tag{6}$$

depending on the energy of an incoming particle and the time at which it exits. Here τ_α is the time a particle spends for a single round trip along the circular edge state of the mesoscopic capacitor. Due to the time-dependent potential, a particle picks up a phase $\Phi_\alpha^q(t) = \frac{e}{\hbar}\int_{t-q\tau_\alpha}^{t} \mathrm{d}t' U_\alpha(t')$, in addition to the phase due to the guiding center motion $qE\tau_\alpha$. The scattering matrix of the full system also depends on the central QPC and the Mach–Zehnder interferometers. A phase is accumulated depending on whether a particle comes from the source $\alpha = A, B$ and whether it traverses the upper or the lower arm of the interferometer $\beta = \mathrm{L}, \mathrm{R}$. This phase is determined by the time for the traversal of the respective interferometer arm and by the magnetic flux. Here we discuss the case of slow driving, meaning that the frequency Ω is much smaller than τ_α^{-1}, but importantly *without requesting restrictions on* Ω *with respect to the time scales related to the entire system.* This means that the traversal times of the interferometer arms can be long with respect to the time scale set by the driving frequency.

If the difference in the path lengths of the interferometer arms is bigger than the spreading of the wave packets emitted by a driven capacitor, *single-particle* interferences in the current are suppressed. We characterize this arm-length difference by the differences in the traversal times τ_L and τ_R. Still in this case, *two-particle* correlations can be observed in the noise properties. We calculate the symmetrized zero-frequency noise power (shot noise) $\mathcal{P}_{12}$ for currents flowing into contacts 1 and 2 in the regime where only two-particle correlations are possibly occurring. If the arm-length differences of the MZIs are chosen to be commensurate, $\Delta\tau := \Delta\tau_\mathrm{L} = \mp\Delta\tau_\mathrm{R}$, we find at zero temperature

$$\begin{aligned}\mathcal{P}_{12} = -\mathcal{P}_0 \sum_{s=\mathrm{e,h}} \{ & T_\mathrm{L} T_\mathrm{R}[1 - L(\Delta t^s)] \\ & - \gamma_\mathrm{L}\gamma_\mathrm{R} \cdot \cos(\Phi_\mathrm{L} \pm \Phi_\mathrm{R})[L(\Delta t^s - \Delta\tau) + L(\Delta t^s + \Delta\tau)]\},\end{aligned} \tag{7}$$

with the parameters T_β and γ_β containing the MZI transmission amplitudes. Here the time difference Δt^s depends on the emission times of electrons $s = e$ and holes $s = h$ from the different single-particle sources and the time delay due to the asymmetry of the setup.

Therefore, Δt^s contains information on the time difference with which particles from the two sources arrive at the interferometer entrances. This time difference enters the Lorentzians, defined by $L(X) = 4\Gamma_A\Gamma_B/[X^2 + (\Gamma_A + \Gamma_B)^2]$, where Γ_A and Γ_B are the widths of the current pulses emitted from the capacitors A and B.

The contribution in the second line in the expression for $\mathcal{P}_{12}$ depends on the magnetic flux. It is different from zero whenever the emission times of the cavities are such that a collision of two electrons (and/or two holes) can take place at the interferometer outputs, $|\Delta t^s \pm \Delta\tau| \leqslant \Gamma_\beta$. It is due to the commensurability of the arm lengths that the collisions taking place at one interferometer output automatically imply the collision at *both* interferometers. The result is an appearance of non-local two-particle correlations irrelevant to the current but with a pronounced effect in the noise. In other words, the two-particle correlations manifest themselves as an AB effect in the noise.

In figure 5 we show the shot noise for $\Delta\tau_{\rm L} = \Delta\tau_{\rm R}$, as a function of the magnetic flux difference and the phase shift φ between the potentials $U_A(t) = U_A\cos(\Omega t)$ and $U_B(t) = U_B\cos(\Omega t + \varphi)$. The tunable phase shift between the modulated potentials yields the difference of emission times from the two capacitors. At $\varphi = \varphi_0$ the condition $\Delta t^e - \Delta\tau = 0$ is satisfied, and an electron emitted by the capacitor A and moving along the lower arm of an interferometer can collide (overlap) with an electron emitted by the capacitor B and moving along the upper arm of the same interferometer (vice versa for $\varphi = -\varphi_0$). Therefore, the which-path information is lost and as a consequence two-particle correlations appear between particles at different contacts. Note that the necessary collisions take place at distant interferometers and in general at different times. Therefore, a variation of the phase difference between the driving potentials can switch on or switch off the two-particle AB effect, by avoiding or allowing collisions. Note that the dip at $\varphi = 0$ is due to fermionic correlations appearing when particles collide at the central QPC, as already discussed for the setup in figure 3. This is the case if $\Delta t^s = 0$ and the first contribution to $\mathcal{P}_{12}$ is suppressed.

In an appropriate time interval, i.e. in the time intervals in which the which-path information is erased, the concurrence

$$C = \frac{2T_C R_C\sqrt{T_{\rm R}^l R_{\rm L}^l T_{\rm L}^l R_{\rm R}^l}}{T_C^2 T_{\rm R}^l R_{\rm L}^l + R_C^2 T_{\rm L}^l R_{\rm R}^l} \tag{8}$$

reaches a maximum. Depending on the QPC transmissions of the middle QPC, T_C, and the transmissions of the different QPCs of the MZIs, $T_{\rm R}^l$, $T_{\rm L}^l$, $T_{\rm L}^l$, $T_{\rm R}^l$, the concurrence reaches the value 1. Importantly, the distinction discussed before between reduced and projected entanglement is not useful in the case of single-particle emitters. One can equally show that a Bell inequality is violated [32], proving the existence of time-bin entanglement. This means that the tunability of the single-particle sources allows us in a controllable way to produce orbitally entangled electrons in given time bins.

Acknowledgments

The authors acknowledge financial support from the Swiss NSF, MaNEP, the ITN NanoCTM and the Ministry of Innovation NRW.

References

[1] Aharonov Y and Bohm D 1959 *Phys. Rev.* **115** 485
[2] Büttiker M, Imry Y and Landauer R 1983 *Phys. Lett.* A **96** 365
Gefen Y, Imry Y and Azbel' M Ya 1984 *Phys. Rev. Lett.* **52** 129

Büttiker M, Imry Y and Azbel' M Ya 1984 *Phys. Rev.* A **30** 1982
Büttiker M, Imry Y, Landauer R and Pinhas S 1985 *Phys. Rev.* B **31** 6207
[3] Webb R A, Washburn S, Umbach C P and Laibowitz R B 1985 *Phys. Rev. Lett.* **54** 2696
[4] Hanbury Brown R and Twiss R Q 1956 *Nature (London)* **178** 1046
[5] Hong C K, Ou Z Y and Mandel L 1987 *Phys. Rev. Lett.* **59** 2044
[6] Büttiker M 1990 *Phys. Rev. Lett.* **65** 2901
Büttiker M 1992 *Phys. Rev.* B **45** 3807
[7] Martin Th and Landauer R 1992 *Phys. Rev.* B **45** 1742
[8] Oliver W D, Kim J, Liu R C and Yamamoto Y 1999 *Science* **284** 299
[9] Henny M, Oberholzer S, Strunk C, Heinzel T, Ensslin K, Holland M and Schnenberger C 1999 *Science* **284** 296
Oberholzer S, Henny M, Strunk C, Schnenberger C., Heinzel T, Ensslin K and Holland M 2000 *Physica* E **6** 314
[10] Fölling S, Gerbier F, Widera A, Mandel O, Gericke T and Bloch I 2005 *Nature* **434** 481
[11] Schellekens M, Hoppeler R, Perrin A, Viana Gomes J, Boiron D, Aspect A and Westbrook C I 2005 *Science* **310** 648
[12] Yurke B and Stoler D 1992 *Phys. Rev.* A **46** 2229
[13] Ji Y, Chung Y, Sprinzak D, Mahalu D, Shtrikman H and Heiblum M 2003 *Nature* **422** 415
Roulleau P, Portier F, Roche P, Cavanna A, Faini G, Gennser U and Mailly D 2008 *Phys. Rev. Lett.* **100** 126802
Litvin L V, Helzel A, Tranitz H-P, Wegscheider W and Strunk C 2008 *Phys. Rev.* B **78** 075303
Bieri E, Weiss M, Göktas O, Hauser M, Schönenberger C and Oberholzer S 2009 *Phys. Rev.* B **79** 245324
[14] Samuelsson P, Sukhorukov E V and Büttiker M 2004 *Phys. Rev. Lett.* **92** 026805
[15] Neder I, Ofek N, Chung Y, Heiblum M, Mahalu D and Umansky V 2007 *Nature* **448** 333
[16] Samuelsson P, Neder I and Büttiker M 2009 *Phys. Rev. Lett.* **102** 106804
[17] Samuelsson P, Neder I and Büttiker M 2009 *Phys. Scr.* T **137** 014023
[18] Büttiker M 1991 *Physica* B **175** 199
Büttiker M 1992 *Phys. Rev. Lett.* **68** 843
[19] Retzker A, Aharonov Y, Botero A, Nussinov S and Reznik B 2006 *Phys. Rev.* A **73** 032106
[20] Mehta P, Samuel J and Sinha S 2010 arXiv:1002.1547
[21] Fève G, Mahé A, Berroir J-M, Kontos T, Plaçais B, Glattli D C, Cavanna A, Etienne B and Jin Y 2007 *Science* **316** 1169
[22] Gabelli J, Fève G, Berroir J-M, Plaçais B, Cavanna A, Etienne B, Jin Y and Glattli D C 2006 *Science* **313** 499
[23] Ol'khovskaya S, Splettstoesser J, Moskalets M and Büttiker M 2008 *Phys. Rev. Lett.* **101** 166802
[24] Splettstoesser J, Ol'khovskaya S, Moskalets M and Büttiker M 2008 *Phys. Rev.* B **78** 205110
[25] Splettstoesser J, Moskalets M and Büttiker M 2009 *Phys. Rev. Lett.* **103** 076804
[26] Blanter Ya M and Büttiker M 2000 *Phys. Rep.* **336** 1
[27] Wootters W K 1998 *Phys. Rev. Lett.* **80** 2245
[28] Beenakker C W J 2006 *Proc. Int. School Phys. E Fermi* vol 162 (Amsterdam: IOS Press)
[29] Prêtre A, Thomas H and Büttiker M 1996 *Phys. Rev B.* **54** 8130
[30] Büttiker M 1986 *Phys. Rev.* B **33** 3020
Büttiker M 1988 *IBM J. Res. Dev.* **32** 63
de Jong M J M and Beenakker C W J 1996 *Physica* A **230** 219
Pilgram S, Samuelsson P, Förster H and Büttiker M 2006 *Phys. Rev. Lett.* **97** 066801
Roulleau P, Portier F, Roche P, Cavanna A, Faini G, Gennser U and Mailly D 2009 *Phys. Rev. Lett.* **102** 236802
[31] Moskalets M, Samuelsson P and Büttiker M 2008 *Phys. Rev. Lett.* **100** 086601
[32] Bell J S 1966 *Rev. Mod. Phys.* **38** 447
Glauber G J 1963 *Phys. Rev.* **130** 2529
Clauser J F, Horne M A, Shimony A and Holt R A 1969 *Phys. Rev. Lett.* **23** 880
Clauser J F and Shimony A 1978 *Rep. Prog. Phys.* **41** 1881